Journal of The Electrochemical Society

The Electrochemical Society
Advancing solid state & electrochemical science & technology

OPEN ACCESS

Evaluation of Redox Chemistries for Single-Use Biodegradable Capillary Flow Batteries

Evaluation of Redox Chemistries for Single-Use Biodegradable Capillary Flow Batteries

Omar A. Ibrahim,[a] Perla Alday,[b] Neus Sabaté,[b,c] Juan Pablo Esquivel,[b,d] and Erik Kjeang[a,*,z]

[a]*Fuel Cell Research Laboratory (FCReL), School of Mechatronic Systems Engineering, Simon Fraser University, Vancouver, Canada*
[b]*Instituto de Microelectrónica de Barcelona, IMB-CNM (CSIC), Campus UAB, Barcelona, Spain*
[c]*Institució Catalana de Recerca i Estudis Avançats (ICREA), Barcelona, Spain*
[d]*Department of Bioengineering, University of Washington, Seattle, Washington 98105, USA*

The rate of battery waste generation is rising dramatically worldwide due to increased use and consumption of electronic devices. A new class of portable and biodegradable capillary flow batteries was recently introduced as a solution for single-use disposable applications. The concept utilizes stored organic redox species and supporting electrolytes inside a dormant capillary flow cell which is activated by the dropwise addition of aqueous liquid. Herein, various organic redox species are systematically evaluated for prospective use in disposable capillary flow cells with regards to their electrochemical characteristics, solubility, storability and biodegradability. Qualitative ex-situ techniques are first applied to assess half-cell solubility, redox potential and kinetics, followed by quantitative in-situ measurements of discharge performance of selected redox chemistries in a microfluidic cell with flow-through porous electrodes. Para-benzoquinone in oxalic acid and either hydroquinone sulfonic acid or ascorbic acid in potassium hydroxide are identified for the positive and negative half-cells, respectively, yielding a maximum discharge power density of 50 mW/cm^2. A prototype capillary flow battery using the same redox chemistries demonstrates robust cell voltages above 1.0 V and maximum discharge power of 1.9 mW. These results show that practical primary battery performance can be achieved with biodegradable chemistries in a disposable device.

Manuscript submitted June 21, 2017; revised manuscript received August 4, 2017. Published August 18, 2017. This was Paper 80 presented at the San Diego, California, Meeting of the Society, May 29- June 2, 2016.

The market demand for small-size single-use electronic devices such as portable sensors and diagnostic devices has been rising drastically in recent years. The power needs of such devices have so far been met by Li-ion batteries and other primary battery technologies, resulting in a consequent rise in their consumption. These batteries often contain heavy metals and strong electrolytes which make them one of the most hazardous components of electronic waste.[1] In addition, the majority of the primary Li batteries used globally are not recycled nor properly disposed of, thus ending up in landfills without regulations.[2] In applications that do not require long discharge times and have modest capacity requirements such as medical devices, these batteries are not even fully discharged before being disposed of. This requires further resources for re-extracting the materials if not recovered, which is not sustainable and raises concerns about the abundance of these resources. The end-of-life fate of these batteries and their life cycle assessment therefore only justifies the use in rechargeable applications beyond hundreds of cycles.[3,4] These issues trigger a worrying concern about associated future environmental hazards from the battery waste generation and urgently call for novel alternatives, tightened environmental policies and switching the linear consumption habit of "take-make-dispose" for these primary batteries into a circular economy model. This approach utilizes novel concepts such as green electronics and cradle-to-cradle design to eliminate waste from the conception of new devices as a top priority considering the waste hierarchy.[5,6]

A few prototypes have been reported to date for batteries that align with the philosophy of green electronics. However, most of these prototypes were designed for transient implantable or edible applications and were generally based on benign metals that will dissolute upon use in a short time. Kim et al. utilized melanin and activated carbon in water activated sodium ion batteries that are edible.[7] Yin et al. discussed the use of biodegradable metals such as Mg, Fe, W or Mo as electrode materials for ingestible applications.[8] Tsang et al. reported the design, fabrication and testing of a biodegradable battery based on Mg and Fe with power output of 30 μW that satisfies the lower range required for implantable applications.[9] Recently, Nadeau et al. demonstrated an ingestible battery based on Zn and Cu that is activated by gastric fluid.[10] Aside from the implantable applications, a biodegradable super capacitor was recently reported as an environmentally friendly energy storage solution.[11]

Various other electrochemical power source concepts have been proposed as sustainable alternatives for portable applications, with limited attention to their end of life disposal. Within the fuel cells category, different organic liquid fuels were used as benign fuel, such as methanol, formic acid, ethanol or ethylene glycol.[12–15] For example, Esquivel et al. presented a paper-based direct methanol fuel cell that can be integrated within lateral flow test strips.[15] However, the electrochemical reactions involving these organic liquid fuels often require precious metal catalysts such as platinum or palladium that are scarce and thus not readily disposable. Other works reported the use of biological fuels, such as glucose.[16–19] However, despite the high energy density associated with biofuels,[18] their power output is generally much lower than the target application requirements and the biocatalysts often have limited stability.[20] Moreover, ion exchange membranes associated with conventional fuel cells are typically not suitable for disposable applications, due to their cost and composition. This dictates the use of membrane-less cell designs such as those recently developed based on co-laminar flow, wherein the mixing of reactants is governed by slow, cross-stream diffusion in lieu of a physical barrier or membrane otherwise used to separate the reactants.[21,22] These membrane-less devices thus offer advantages in cost, simplicity, performance and durability.[23] In addition, membrane-less cells have the flexibility of tuning the specific conditions in each half-cell (mixed-media operation) since the conditions are not restricted by the ion selective membranes required in conventional cells.[24] Kjeang et al. applied flow through porous electrodes in co-laminar flow cells, which eliminated mass transport limitations and enabled full utilization of the three dimensional electrode area for increased reactant conversion and high discharge power density.[25] These porous electrodes were recently engineered together with the device dimensions to offer unprecedented power densities of 2.0 W/cm^2, which is the highest performance reported to date for aqueous electrochemical flow cells.[26]

*Electrochemical Society Member.
[z]E-mail: ekjeang@sfu.ca

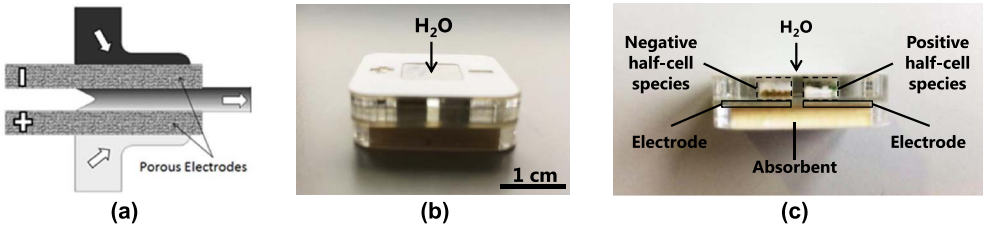

Figure 1. a) Microfluidic co-laminar flow cell with flow-through porous electrodes used for measuring discharge performance. b) Side view and c) cross-sectional view of the disposable capillary flow cell used for final demonstration of reactant chemistries in an integrated device.

Nevertheless, the vanadium redox electrolyte used in that case is not adequate for single-use applications, due to associated toxicity and cost.

Many paper-based electrochemical cells have been reported owing to various advantages such as self-pumping using capillarity, simplicity, disposability enabled by low-cost and ease of integration within devices for low-resource environments.[27,28] In the case of co-laminar flow cells, the capillary action in paper-based cells can eliminate the need for a pump to drive the flow.[15] Some paper-based devices relied on the use of metals such as Cu, Al, Mg or Ag to form a microfluidic galvanic cell,[29,30] with open circuit voltages up to 2.2 V.[31] Others have developed biological and microbial fuel cells in paper.[32,33] Choi et al. presented various bio-fuel cells in a paper platform as an alternative power source based on benign fuel alternatives that can be harvested.[34–36] Lee and Choi presented an origami paper based bacterial battery with a power output of 48 nW.[37] Other researchers utilized Li-ion origami-inspired paper batteries for both transient and rechargeable uses.[38–40]

Recently, a new concept of single-use capillary flow batteries was introduced, which can be disposed of by the biotic degradative process.[41] This allows the battery to close its life cycle to nature at its end-of-life, which complies well with the circular economy and the concepts of green electronics as the associated waste is minimized from the device conception. The concept leverages advances in paper-based fuel cells which enable self-pumping and microfluidic fuel cells with flow–through porous electrodes which enable high power densities. The battery is made exclusively of environmentally benign, biotically degradable materials such as cellulose and beeswax. The electrochemical energy conversion utilizes organic redox reactants which are stored on the device in solid phase in a dedicated compartment. Upon activation by the dropwise addition of liquid, the stored reactants and electrolytes dissolve and flow by capillarity through the pore network of the electrodes where the power is generated.

In this work, various organic redox species are systematically analyzed and evaluated for prospective use in disposable capillary flow cells. The chemistry requirements for this class of batteries are reviewed with regards to their electrochemical characteristics, solubility, storability and biodegradability, and the results for the evaluation of redox reactants and electrolytes, suitable for the operation of the disposable device, are presented. The investigation includes half-cell assessment of the redox reactants and electrolytes regarding their redox potential and kinetics as well as cell level assessment to measure their discharge performance. Finally, the identified chemistries are demonstrated in an integrated capillary flow cell.

Experimental

Sulfuric acid (H_2SO_4, 95%) from Caledon Laboratories Ltd (Georgetown, ON, Canada) is diluted to the desired concentrations (0.5–1 M). Leucoquinizarin (LQ) is purchased from TCI America (Portland, OR, USA) and used as received. All other species and electrolytes are purchased from Sigma Aldrich (Oakville, ON, Canada), and used as received, unless otherwise stated.

The redox chemistry screening is based on identifying suitable redox species and supporting electrolytes that are commercially available, aided by literature. Solutions are prepared by dissolving each combination of supporting electrolyte and redox species, consecutively, in deionized water (DI-H_2O, Millipore) to the desired concentrations. The solubility of the species is assessed in water and/or desired electrolytes based on literature and on visual absence of solid precipitation at the desired concentrations. The soluble redox chemistry options are then characterized ex-situ using voltammetry techniques to measure the open circuit potential (OCP) and to qualitatively assess the electrochemical reaction kinetics for the different redox species and electrolytes. The measurements are performed in a conventional three-electrode electrochemical cell bubbled with nitrogen to minimize solution oxidation due to dissolved oxygen or ambient air. Glassy carbon electrode (0.07 cm^2), platinum wire electrode and saturated calomel electrode (SCE) (CH instruments Inc, TX, USA) are used as working electrode, counter electrode and reference electrode, respectively, and the cell is operated by a frequency response analysis compatible potentiostat (Gamry, Reference 3000). Prior to scanning, the OCP of each half-cell is measured at zero applied current. Cyclic voltammetry (CV) is then recorded at a scan rate (ω) of 50 mV/s followed by linear sweep voltammetry (LSV) measurements in the voltage sweep direction of the respective discharge reaction of interest at various scan rates of 5, 10, 25, 50 and 100 mV/s. The cell ohmic resistance is measured by means of electrochemical impedance spectroscopy (EIS) performed using the same potentiostat from 1 MHz to 1 Hz with an AC amplitude of 10 mV rms at the OCP, by reading the high frequency real axis intercept value of the Nyquist plot. The resistance value obtained is used to perform post-measurement IR-compensation of the measured voltammograms.

Next, the discharge performance of the selected redox chemistries is measured in-situ in a microfluidic co-laminar flow cell.[23] A microfluidic cell design with flow through porous electrodes[25] is used as an analytical platform for the in-situ discharge performance analysis, as shown in Fig. 1a. The cell design was previously used in other analytical studies and shown to enable high discharge performance and minimal cross over losses.[42] The device is fabricated by UV soft lithography of polydimethylsiloxane (PDMS) (Dow Corning) from an SU-8 (Microchem) photoresist master with 150 μm height then bonded to a glass slide. Rectangular strips of carbon paper (TGPH-060, Toray), with 1 mm width, are heat treated and placed to form both cell electrodes. Further details about the device design and fabrication can be found elsewhere.[43] The pre-mixed solutions of redox reactants and supporting electrolytes are prepared at required concentrations and pumped into the cell by means of a dual syringe pump (Harvard apparatus) at a flow rate of 10 or 100 μL/min. This flow rate is chosen in order to minimize influences from mass transport losses on the cell performance, as demonstrated in other works utilizing the same analytical cell.[42] The measurements are performed by the same potentiostat in potentiodynamic mode at a scan rate that is slow enough to match steady state measurements (10 mV/s) from OCP to 0.1 V. The performance is normalized to the active cross sectional area normal to the flow (0.5 $\times$ 0.015 cm^2). The cell ohmic resistance is measured by EIS performed at OCP using the same potentiostat and same frequency range as in the ex-situ measurements.

Finally, the identified suitable redox species and supporting electrolytes are tested in a disposable capillary flow cell featuring the same design as the biodegradable battery recently reported,[41] wherein the reactant and electrolyte species are stored on the device in solid form,

Table I. Structure, standard potential and theoretical capacity of basic quinone compounds.

Quinone (CAS no.)	1,4-Benzoquinone (106–51-4)	1,2-Benzoquinone (583-63-1)	1,4-Naphtoquinone (130-15-4)	9,10-Anthraquinone (84-65-1)
Structure			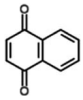	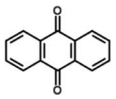
Abbreviation	pBQ	oBQ	NQ	AQ
Standard potential (vs. SHE)	0.69 V	0.78 V	0.48 V	0.15 V
Theoretical capacity (mAh/g)	496	496	339	257

as shown in Fig. 1b and Fig. 1c. In this case, the device enclosure is made of PET-based pressure sensitive adhesives (PSA) (Adhesives Research, Glen Rock, PA, USA) and poly (methyl methacrylate) (PMMA) layers, for rapid prototyping using CO_2 laser micromachining (Mini 24, Epilog Laser, Golden, CO, USA). Cellulose paper (Ahlstrom, Helsinki, Finland) is laser cut and used for absorbent pads to provide the capillary flow. Porous carbon paper strips (TGPH-120, Toray) are heat treated and used as electrodes with an active area of 0.25 cm^2. Further details about the device fabrication and structure can be found elsewhere.[41] The device is activated by adding 1 mL of DI-H_2O and the OCP is monitored for 1 hour. During this measurement period, a cell polarization curve is measured and recorded every 5 minutes in potentiodynamic mode from OCP to zero volts.

Reactant Chemistry Requirements and Selection

A disposable capillary flow battery resembles a redox flow battery albeit of a primary battery type designed for single-use discharge operation. This new class of batteries features unique requirements for the redox chemistries used in the positive and negative half-cells. The opportunity enabled by the capillary flow cell design is to achieve a fully biodegradable device with high performance and stability. The active redox species used as reactants are therefore required to exist in the solid phase at ambient conditions, for instance in powder form, to enable 'dormant' storage on the cell with useful shelf life. They should moreover be soluble in water or other desired electrolytes such that they dissolve upon liquid activation of the device and are carried into the flow-through porous electrodes for the electrochemical energy conversion. They are also required to be biodegradable and thus preferably organic. The species should also be stored on the cell in the correct redox state required for discharge operation with net current generation at an adequate cell voltage. Furthermore, their electrochemical reactions should be compatible with catalyst-free carbon electrodes with fast kinetics.

The use of organic active redox species is an emerging alternative for redox flow battery development[44–46] and has recently captured the interest of the energy storage research community.[47–50] Huskinson et al. introduced a novel flow battery system for energy storage, in which they coupled a quinone redox species with a bromine positive half-cell. Their metal-free cell showed high power density during discharge and high cycling efficiency.[47] Yang et al. substituted the toxic bromine with another, high-reduction potential quinone, to create an ecofriendly, water-based all-quinone system and named it the organic redox battery (ORBAT).[48] Quinones are inexpensive and can be extracted from natural organic compounds present in plants, which makes them eco-friendly. Moreover, quinone redox species generally have rapid kinetics on catalyst-free carbon electrodes.

Quinone compounds can generally be defined as a class of cyclic organic compounds that contain two carbonyl groups (C = O). This class includes for example benzoquinones, naphthoquinones and anthraquinones, as the basic forms shown in Table I. By the addition of more rings to the structure, the aqueous solubility and standard reduction potential are expected to decrease,[51] as shown in Table I. Therefore, benzoquinones (BQ) will have the highest solubility and highest standard potential while anthraquinones (AQ) will have the least solubility and the lowest standard potential. Alternatively, naphtoquinones (NQ) are expected to have moderate solubility and standard reduction potential between BQ and AQ and may therefore also be considered. These quinone compounds can moreover be tuned for their standard reduction potentials as well as their solubility by adding different functional groups to the structure.[50,52] When quinones are reduced reversibly to their respective hydroquinones, the two carbonyl groups change to two hydroxyl groups (C−OH). Their electrochemical reactions involve two electrons in either acidic[47,48] or alkaline conditions,[45,49] as shown in Eqs. 1–2, respectively.

$$\text{Acidic conditions:} \quad Q_a + 2\,\bar{e} + 2\,H^+ \Leftrightarrow H_2Q_a \qquad [1]$$

$$\text{Alkaline conditions:} \quad Q_b + 2\,\bar{e} \Leftrightarrow {Q_b}^{2-} \qquad [2]$$

In addition, quinones have high probability of fast biodegradation as predicted by the biodegradation models (BIOWIN) in EPISuite and other works.[53,54] The quinone species are therefore considered to satisfy the majority of the disposable battery criteria. A preliminary discharge experiment in a microfluidic cell is therefore conducted to establish a proof-of-concept for the all-quinone chemistry. The reactants in this example are adopted from the ORBAT[48] and includes using sodium salts of anthraquinone-2-sulfonic acid (AQS, Fig. 2a) and 1,2-dihydroxybenzene 3,5-disulfonic acid (H_2BQDS, Fig. 2b) as negative and positive half-cells, respectively, in 1 M sulfuric acid (H_2SO_4). While H_2BQDS has relatively high solubility due to the hydroxyl (−OH) and sulfonic acid ($-SO_3^-$) groups, the solubility of the sodium salt of AQS is merely ~0.05 M. Therefore, solutions of H_2BQDS and AQS are prepared and tested at a concentration of 0.05 M in 1 M H_2SO_4. In order to perform in-situ battery discharge performance measurements, the solutions are first electrolytically charged to the forms required for discharge in a separate, custom made flow cell at 1.0 V applied voltage. After charging, the AQS is reduced into

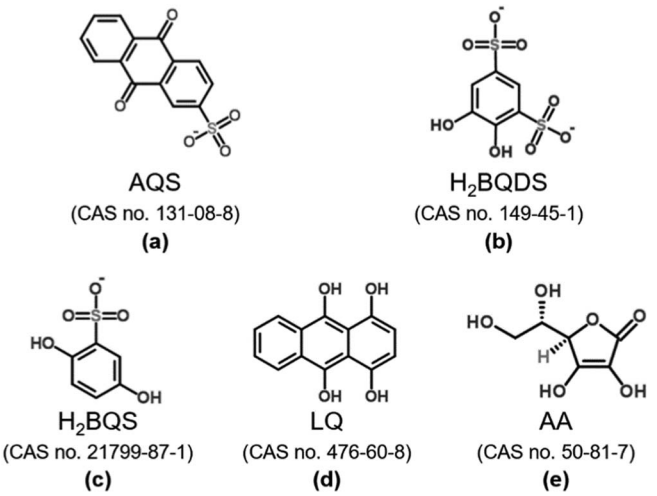

Figure 2. Structures of quinones used in ORBAT[48] (a, b) and this work (c, d, e).

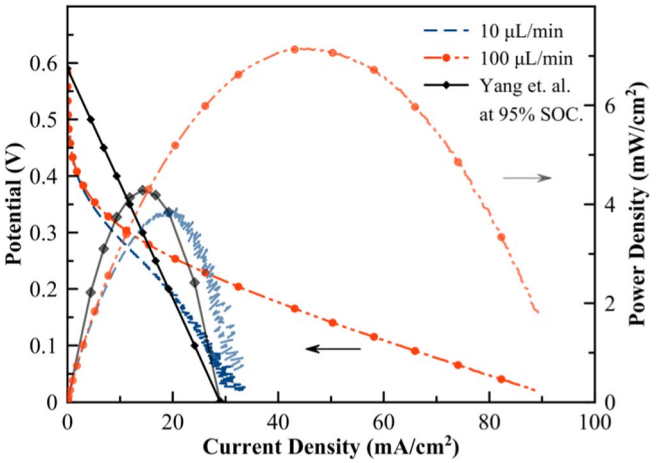

Figure 3. Discharge results in a microfluidic co-laminar flow cell for the all-quinone battery chemistry with H_2BQDS and AQS based on ORBAT compared with discharge data at 95% SOC from literature.[48]

H_2AQS and the H_2BQDS is oxidized into BQDS, both of which are suitable for discharge experiments in the microfluidic cell. This is confirmed by the change of color from light yellow to dark green in the case of AQS/H_2AQS and from a colorless solution to light brown in case of H_2BQDS/BQDS, which is consistent with literature.[55,56] The results of the discharge experiments in the microfluidic cell operated at flow rates of 10 and 100 μL/min are shown in Fig. 3. The cell is found to have an OCP of 0.59 V and a peak power density of 3.9 mW/cm^2 at 10 μL/min, which is in good agreement when compared with a linear approximation of the discharge data reported for the ORBAT at 95% state-of-charge (SOC).[48] At the high flow rate of 100 μL/min, the cell output is increased to 7.2 mW/cm^2 because of the enhanced mass transport at higher flow rates.

The limited solubility of AQS can be improved by applying a sodium ion exchange step, and thus higher associated discharge performance outputs can be anticipated, as shown in other works.[57] Nonetheless, the commercially available forms of these quinone compounds are generally in a redox state that cannot be directly used for discharge, as an initial charging step would be required. To elaborate this challenge on the demonstrated example above, the high potential quinone intended for the positive half-cell is available commercially in its reduced form (e.g., Tiron or H_2BQDS) while the low potential quinone intended for the negative half-cell is available in the oxidized form (AQS). In order to store the species on the disposable cell in a redox state ready for discharge, the positive half-cell requires a high potential species in an oxidized/quinone form (= O), while the negative half-cell requires a low potential species in a reduced/hydroquinone form (−OH).

In order to overcome the challenge of the desired redox state of the quinone compounds for direct use in discharge operation, the pH dependence of the standard redox potential of quinones can be leveraged in the present application.[58,59] This is facilitated by mixed-media operating conditions in which an alkaline negative electrode and an acidic positive electrode are employed. This enables higher electrochemical cell voltages during discharge operation and hence the available reduced quinones (−OH) can be used under alkaline conditions at the negative electrode for direct discharge operation. This mixed-media feature is uniquely enabled by membrane-less cells such as the microfluidic co-laminar flow cells where the diffusion interface is used to separate the reactant streams instead of a physical barrier such as ion exchange membranes which dictate the choice of the reactant media. For the present application, the mixed-media condition not only enables higher cell voltage but also enables utilization of a wider range of commercially available species and electrolytes. Furthermore, mixed-media operation offers an opportunity for the acidic and alkaline electrolytes to neutralize downstream by means of diffusive mixing to form neutral or near neutral pH conditions that allow safe disposal, which is an essential requirement for the disposable cell.

A subset of potential organic redox species are identified to theoretically meet all the aforementioned selection criteria of storability, solubility, biodegradability, correct redox state, adequate redox potential and good kinetics. For the oxidized quinone to be used in the positive electrode, para-benzoquinone (pBQ), shown earlier in Table I is identified and selected. pBQ is the most basic form of quinone compounds and is therefore soluble in aqueous media and readily biodegradable. pBQ is also commercially available in solid form in its oxidized state which enables direct use for electrochemical reduction in the positive half-cell of the battery. The choice of pBQ is favored over other oxidized quinones such as NQ and AQ (Table I) since both NQ and AQ have lower solubility and standard reduction potential and are thus considered inadequate for the current application. While the ortho-benzoquinone (oBQ) has higher reduction potential than pBQ, it is not found commercially available in the oxidized form and only the reduced form (Catechol) is available. On the other hand, for the reduced hydroquinones to be used at the negative electrode, hydroquinone sulfonic acid (H_2BQS, Fig. 2c), is an example identified as a potential benzoquinone available in the reduced form. Beside benzoquinones, anthraquinones are known to have relatively low standard potential and are thus considered suitable for use in the negative electrode of the current approach, by facilitating a sufficiently negative electrode potential when used in alkaline media for a targeted cell potential on the order of ∼1 V. The reduced forms of anthraquinones available commercially are limited however, and the most suitable option for the negative half-cell is deemed to be 1,4,9,10-Tetrahydroxyanthracene or leucoquinizarin (LQ, Fig. 2d). In addition to the quinone based species, organic acids with anti-oxidant characteristics can also be considered as biodegradable options for the negative half-cell. For example, ascorbic acid (AA, Fig. 2e), also known as vitamin C, is deemed to be a theoretically viable candidate for the negative half-cell as it is a soluble phytochemical and commonly used antioxidant with a suitably negative standard potential for oxidation.

Results and Discussion

The reactant chemistry options that passed the preliminary screening described in the previous section are experimentally assessed for prospective use in disposable capillary flow batteries according to the aforementioned criteria. The solubility of the species is first assessed in water and/or desired electrolytes. The species are then evaluated ex-situ by measuring their half-cell open circuit potentials (OCPs) and electrochemical kinetics by using cyclic voltammetry (CV) and linear sweep voltammetry (LSV) techniques. Next, the discharge performance is measured in-situ in a microfluidic co-laminar flow cell with flow-through porous carbon electrodes, aiming for a power density output in the range of tens of mW/cm^2. The most promising reactant chemistries are finally demonstrated in a capillary flow cell device.

Ex-situ assessment of viable half-cells.—For the positive half-cell, para-Benzoquinone (pBQ) is first selected for evaluation. It undergoes a two electron, two proton transfer in acidic media, following Eq. 1, with a standard reduction potential of 0.69 V vs. SHE.[60] Here, pBQ is found to have an aqueous solubility limit of 0.1 M at room temperature and is thus dissolved to this saturation concentration in 1 M sulfuric acid (H_2SO_4) as a benchmark acidic supporting electrolyte. The measured half-cell OCP equals 0.52 V vs. SCE, which is in reasonable agreement with the standard potential given the more acidic condition and fully oxidized form used here. The IR-compensated CV of 0.1 M pBQ is shown in Fig. 4a at a scan rate of 50 mV/s. The figure shows a peak current density ratio (i_{pa}/i_{pc}) close to unity but with a relatively wide peak separation ($E_{pa} - E_{pc}$) of 445 mV, which is much greater than the 59 mV per electron expected for a reversible process. While quinones are generally known to be electrochemically reversible in aqueous media, this behavior of pBQ is in

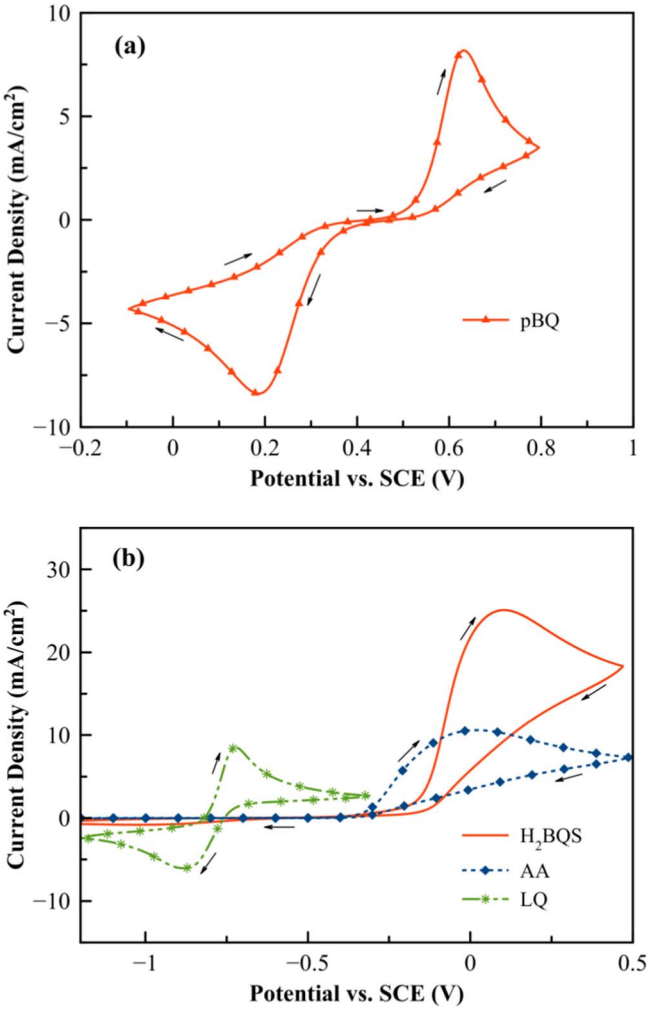

Figure 4. IR-compensated cyclic voltammograms at a scan rate of 50 mV/s for a) 0.1 M pBQ in 1 M H_2SO_4 and b) 0.1 M H_2BQS, AA and LQ in 1 M KOH.

agreement with literature studies where the peak separation is observed to increase in buffered media, indicating an overall process with relatively slow kinetics.[58,59,61] IR-compensated LSVs are shown in Fig. 5a at various scan rates for the respective electrochemical reduction of pBQ of concern to this study. The cathodic peak current densities (i_{pc}) are shown to have approximately linear proportionality with the square root of the scan rate ($\omega^{0.5}$), as shown in the figure inset, indicating a process that is diffusion controlled. The i_{pc} values in this case are higher than for the CV data (Fig. 4a) due to the decrease in cathodic current after each cycle in the CV as it approaches a steady result. The figure also shows that the cathodic peak potential (E_c) varies slightly with the scan rate and that the difference between cathodic peak potential and potential at half peak current ($|E_{pc} - E_{pc/2}|$) decreases with reduced scan rate, which confirm a quasi-reversible process. Overall, pBQ shows good kinetics on the carbon electrode and is deemed an adequate reactant species for the positive half-cell of the present application.

For the negative half-cell, H_2BQS; a hydroquinone, AA; a commonly used antioxidant compound present in nature and LQ; a reduced anthraquinone are identified for potential use, as they exist in the reduced redox state, and are thus evaluated in 1 M potassium hydroxide (KOH) to establish the desired alkaline conditions for this electrode. The electrochemical reaction for the quinones (H_2BQS and LQ) involves transfer of two electrons after deprotonation in alkaline conditions,[49] following Eq. 2. For the AA case, the electrochemical reaction in highly alkaline media also follows Eq. 2 and involves a two electron oxidation of ascorbate,[62,63] since deprotonation of the acid occurs by reaction with KOH. The solubility in aqueous media is found to be much higher for H_2BQS and AA than for the pBQ previously assessed for the positive half-cell. H_2BQS is soluble up to 0.7 M while AA is soluble up to 1.9 M in water. However, LQ is found to be poorly soluble in water and to have a hydrophobic behavior, which may impose a limitation for the present application. The solubility limit for the three compounds is expected to be particularly high in KOH solution due to the deprotonation that provides solubility and higher electron donation capabilities.[49] The three compounds are however further evaluated at a concentration of only 0.1 M in 1 M KOH in order to match the concentration of the corresponding pBQ in the other half-cell and thereby balance the overall cell chemistry. Next, the three redox species are characterized ex-situ using the voltammetry techniques, while nitrogen is bubbled into the cell to minimize solution partial oxidation[56] by dissolved oxygen or ambient air and enhance stability. Before the potential sweep, the

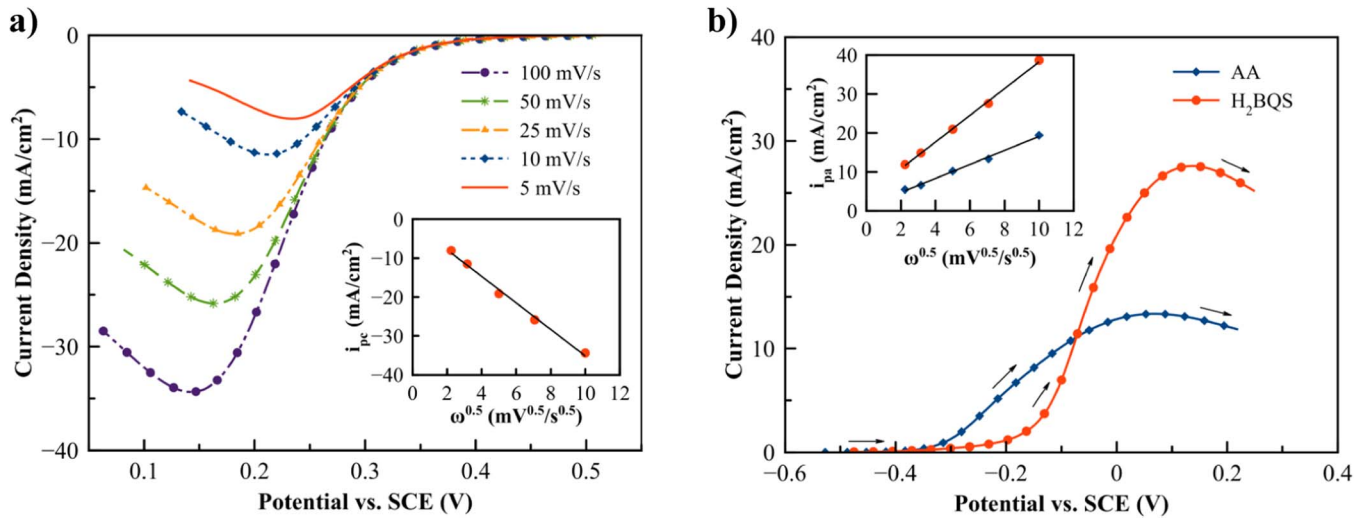

Figure 5. IR-compensated linear sweep voltammograms representing the a) electrochemical reduction of 0.1 M pBQ in 1 M H_2SO_4 at various scan rates and b) electrochemical oxidation of 0.1 M H_2BQS and AA in 1 M KOH at a scan rate of 50 mV/s. The figure insets show the peak current densities (i_p) versus the square root of the scan rates ($\omega^{0.5}$).

half-cell OCPs are measured to be −0.47 V, −0.53 V and −0.80 V vs. SCE for the H_2BQS, AA and LQ, respectively, which suggests a prospective full cell potential window of > 1.0 V when paired with pBQ. IR-compensated CVs for the three redox species are shown in Fig. 4b at a scan rate of 50 mV/s. The LQ active species shows a reversible electrochemical process, which was also observed in other works for anthraquinone compounds in alkaline media.[45,49] The CV shows a peak current density ratio (i_{pa}/i_{pc}) of around 1.15 and a peak separation ($E_{pa} - E_{pc}$) of 159 mV. Nevertheless, the LQ is found to be rather unstable and its oxidized form has limited solubility in KOH causing visually observed precipitation which challenges its prospective use in capillary flow cells due to possible clogging of the porous media. Recalling that the active species and supporting electrolytes are intended to be stored in solid form and simultaneously dissolve in water, the LQ is hence deemed unsuitable because of its aqueous solubility limitations and is excluded from operation of the final device.

In contrast to the LQ case, the reverse (cathodic) peak is absent in both cases of AA and H_2BQS. The absence of the reverse peak is likely attributed to the instability of the electro-oxidation produced species in alkaline conditions, as also observed in other works.[61,64–66] Post CV, the half-cell OCP for both species drops below −0.6 V vs. SCE, which suggests the formation and presence of a new species in the solution. Despite these indications that both H_2BQS and AA may not be reversible under alkaline conditions and hence unsuitable for a conventional flow battery application in alkaline conditions, both are still deemed adequate for the primary battery approach presented in this work, since only the electro-oxidation portion of the cycle is of interest. Despite the more positive half-cell OCP of H_2BQS compared to AA which results in a slightly lower cell voltage, the CV results also show that H_2BQS has a higher peak current density than AA which may reflect higher species diffusivity and faster kinetics.

For the anodic (oxidation) peak of interest to the primary battery approach, IR-compensated LSVs for 0.1 M redox active species (AA and H_2BQS) in 1 M KOH are shown in Fig. 5b, at a scan rate of 50 mV/s. Both species exhibit an anodic peak potential (E_{pa}) that varies slightly with the scan rate. Similar to the CV results, the electro-oxidation of H_2BQS has a higher anodic peak current density (i_{pa}) compared to AA, which indicates a higher diffusion rate and faster kinetics. The difference in kinetics of the electro-oxidation can also be observed from the difference of the peak potential and the potential at half peak current density ($E_{pa} - E_{pa/2}$) in each case. For example, at 50 mV/s, this difference equals 193 and 252 mV for H_2BQS and AA, respectively, indicating that H_2BQS has faster kinetics. The anodic peak current densities (i_{pa}) are shown to be approximately proportional to the square root of the scan rate (inset of Fig. 5b), wherein H_2BQS has a higher slope than AA, again reflecting the higher diffusion and faster kinetics. It is thus concluded that both AA and H_2BQS are suitable for the final device application, with AA having a more negative half-cell OCP advantage and H_2BQS having a higher diffusion rate and faster kinetics.

Ex-situ assessment of compatible supporting electrolytes.—In order to satisfy the functional requirements of disposable capillary flow cells, both active species and supporting electrolytes need to be stored in the solid phase onboard the device, for instance in powder form, and then activated by addition of liquid when used for battery discharge. The active redox species selected in the previous section achieve these requirements in full. For the supporting electrolytes, the KOH used as a supporting electrolyte at the negative electrode exists in solid form and thus can also be stored and dissolved on the final device to fulfill the requirements. However, while H_2SO_4 shows high performance when initially used as a benchmark supporting electrolyte at the positive electrode, it cannot be dried or stored in the solid phase on the final device. Therefore, it needs to be replaced with a suitable supporting electrolyte that is available in solid phase and soluble in aqueous media. Various organic or inorganic acids or salts could be considered for this purpose; however, the resulting supporting electrolyte must also be stable with inert chemical and electrochemical

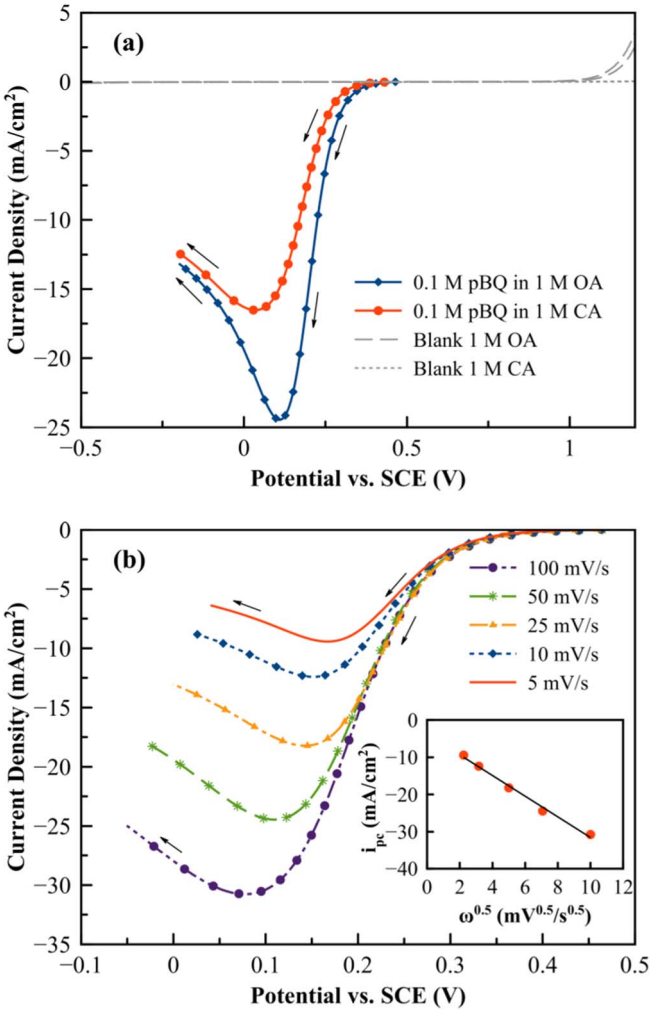

Figure 6. IR-compensated linear sweep voltammograms representing the electrochemical reduction of a) 0.1 M pBQ in 1 M OA and 1 M CA at 50 mV/s with a background CV presenting inert activity for blank supporting electrolytes and b) 0.1 M pBQ in 1 M OA at various scan rates with an inset showing the cathodic peak current density (i_{pc}) versus the square root of the scan rates ($\omega^{0.5}$).

activity, acidic at low pH in order to maintain the mixed-media benefits and have high ionic conductivity in order to retain the good discharge performance. For example, oxalic acid (OA) is identified as a strong organic acid with low measured pH and aqueous solubility up to 1 M. Moreover, citric acid (CA) is also identified as another organic acid with a much higher solubility limit. Both OA and CA are phytochemicals that are present in nature and are both predicted to have fast biodegradation probability by EPISuite from the US Environmental Protection Agency.[54] At a concentration of 1 M, the pH is measured to be in the range of 0.5–1 and 1.5–2 for OA and CA, respectively (pH test paper, Fisher Scientific, ON, Canada). The OCP of 0.1 M pBQ in 1 M OA and in 1 M CA is measured to equal 0.47 and 0.42 vs. SCE, respectively. The relatively low (less positive) half-cell OCP in case of CA supporting electrolyte is likely attributed to the higher pH which results in lower Nernstian potential due to the pH dependence of pBQ standard potential. Moreover, impedance measurements indicate that CA has an order of magnitude higher solution resistance, presumably due to lower dissociation of the acid. The IR-compensated LSVs measured for both cases are shown in Fig. 6a, at a scan rate of 50 mV/s. The data show a lower cathodic peak current density (i_{pc}) for pBQ reduction in CA supporting electrolyte compared to the corresponding result for OA, which is consistent with the previous results and

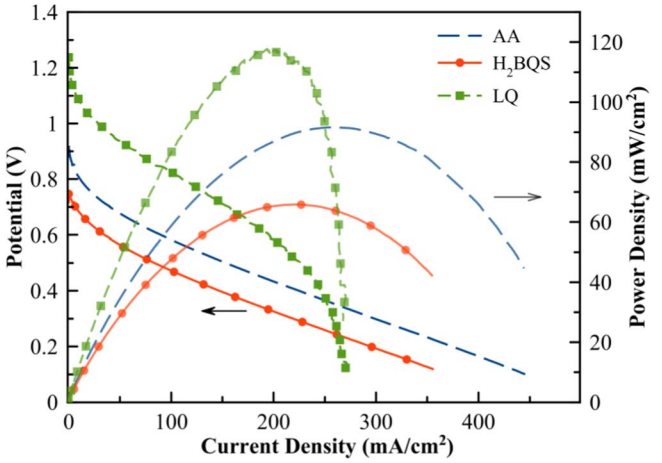

Figure 7. Polarization results of in-situ measurements in a microfluidic co-laminar flow cell operated on 0.1 pBQ in 1 M H_2SO_4 at the positive electrode and 0.1 M AA, H_2BQS and LQ in 1 M KOH at the negative electrode.

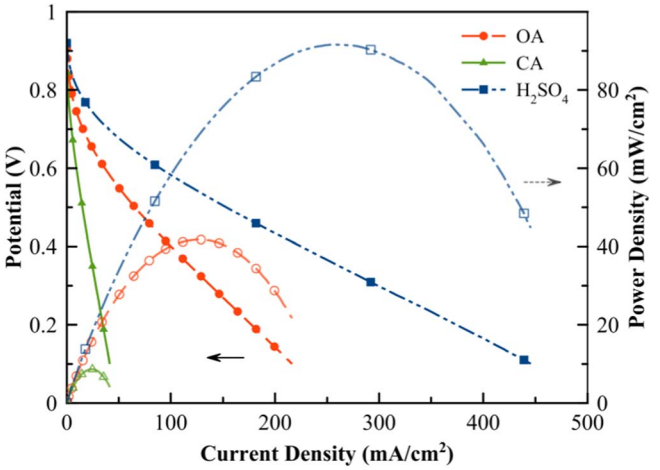

Figure 8. Polarization and power density discharge curves in a microfluidic co-laminar flow cell using 0.1 M AA in 1 M KOH at the negative electrode and 0.1 M pBQ in 1 M H_2SO_4, OA and CA at the positive electrode.

likely due to the lower availability of protons for the pBQ reduction.[64] Blank supporting electrolyte CVs at 50 mV/s are also shown in the background of Fig. 6a, wherein the electro-oxidation of electrolyte species is not expected to occur in the potential range of interest at the catalyst-free electrode materials and conditions of this study,[67] which confirms the inert activity of both CA and OA as supporting electrolytes. Nevertheless, despite the much higher solubility of the CA supporting electrolyte than OA, the latter option is likely preferred due to the more positive potential, faster kinetics and higher ionic conductivity, which are likely to positively impact the cell performance. IR-compensated LSVs for the 1 M OA supporting electrolyte case are shown in Fig. 6b, again representing the electrochemical reduction of 0.1 M pBQ at various scan rates. The results suggest quasi-reversible kinetics in this case, considering the variation of the cathodic peak potential (E_{pc}) and increase of $|E_{pc} - E_{pc/2}|$ with increased scan rates. The linearity of the peak cathodic current density (i_{pc}) with the square root of the scan rates ($\omega^{0.5}$) is also shown in the same figure inset. The result suggests similar reduction kinetics for the OA case when compared to the H_2SO_4 benchmark electrolyte case. For example, at 50 mV/s, the cathodic peak current densities i_{pc} equal −24.5 and −25.8 mA/cm^2, while the measured $|E_{pc} - E_{pc/2}|$ values equal 103 and 83.6 mV, for the OA and H_2SO_4 cases, respectively. However, the OA cell resistance is found to be higher than the H_2SO_4 case due to the lower ionic conductivity[60] which may hence suggest a reduced in-situ discharge performance.

In-situ microfluidic co-laminar flow cell discharge performance.—Next, the in-situ discharge performance is measured, using the resulting positive and negative half-cells together in mixed media operation inside the microfluidic cell with flow-through porous electrodes. A solution of 0.1 M pBQ in 1 M H_2SO_4 is initially used at the positive electrode of the cell and measured against the three negative half-cell options of 0.1 M H_2BQS, AA and LQ in 1 M KOH at the negative electrode. The polarization curves and power density curves for the three cases are shown in Fig. 7, at the flow rate of 100 μL/min. The AA at the negative electrode shows a cell OCP of 0.92 V whereas for H_2BQS, the OCP equals 0.78 V. The EIS measurements show similar cell resistance values around 90 Ω for both cases, a value which is dominated by the ionic resistance of the electrolytes. This is also reflected by the similar slopes in the ohmic region of the polarization curves. The cell achieved peak power densities of 90 and 65 mW/cm^2 for AA and H_2BQS, respectively, which meets and exceeds the present application requirements in both cases. In addition, the result when using LQ is also shown on the same figure wherein the cell achieved a higher OCP of 1.24 V, which to the authors' knowledge represents the highest all-quinone aqueous electrochemical cell potential reported to date. Although a higher power density of 120 mW/cm^2 is measured for the LQ case, higher mass transport limitations are also observed, despite the low reactant utilization at these flow rates. This further confirms the limited stability of LQ and the limited solubility of its oxidation product, as previously indicated in the ex-situ analysis section, which results in potential electrode clogging and limits the prospective use of LQ in the present application. In general, the performance obtained in the microfluidic cell with dilute concentrations of active organic redox species on metal-free electrodes is remarkable. The peak power density achieved is comparable to that of previously reported cell designs based on concentrated liquid organic fuels and precious metal catalysts[13,14] and is several orders of magnitude higher than other environmentally friendly approaches based on biofuel cells.[18,37]

Then, the effect of the supporting electrolytes on the full cell discharge performance is assessed in-situ in the microfluidic co-laminar flow cell, and compared to the H_2SO_4 benchmark case. Fig. 8 presents the polarization curves and power density curves for 0.1 M pBQ in 1 M of the supporting electrolytes of OA and CA coupled with 0.1 M AA in 1 M KOH at the negative electrode. The AA case is chosen here as it showed higher performance than H_2BQS (Fig. 7). The discharge performance for the H_2SO_4 benchmark case is also shown in the same figure for comparison. It is shown that the peak power density with CA is 10 mW/cm^2, which is merely 11% of the discharge power density obtained with H_2SO_4 and further confirms the performance trade-offs of CA observed in the ex-situ study. The cell OCP for the OA case is slightly lower than the benchmark case with H_2SO_4, which is explained by the lower acidity (higher pKa) of OA and higher pH than H_2SO_4. More importantly, however, a peak power density of 42 mW/cm^2 is obtained with OA as supporting electrolyte, which is considered to meet the cell performance requirement of the target portable applications. The combined ohmic cell resistances are measured by means of EIS and are found to be 90, 170 and 1200 Ω for the cases of H_2SO_4, OA and CA, respectively, which explains the much stronger performance in case of OA than that of CA. The result also suggests an ohmic limited cell performance which explains the trade-off of using OA supporting electrolyte when compared to H_2SO_4. While OA allows the possibility of solid phase storage on the final device, it has relatively low ionic conductivity compared to H_2SO_4,[60] which results in increased ohmic cell resistance from 90 to 170 Ω and the consequent reduction in peak power density from 90 to 42 mW/cm^2.

Demonstration in a capillary flow cell.—Finally, the proposed redox chemistries are integrated and tested in a disposable cell design in which the flow is solely provided by capillarity and all redox

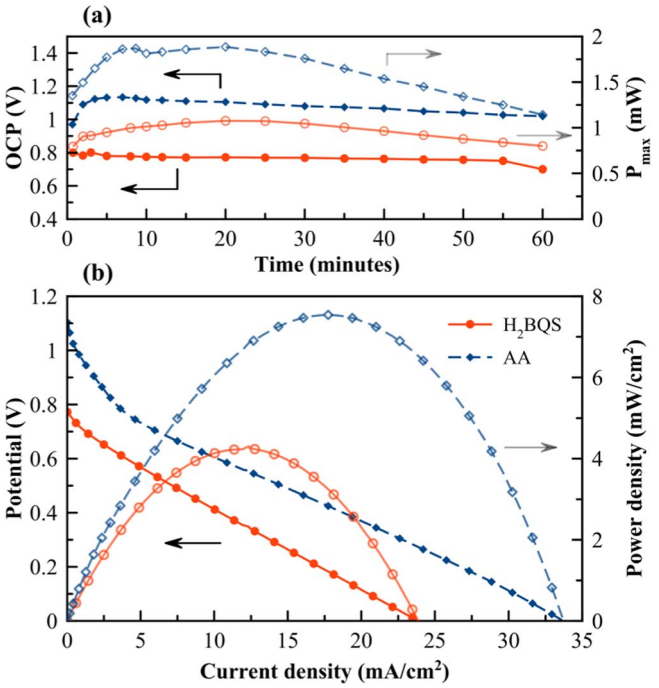

Figure 9. Discharge results for a disposable capillary flow cell device using the selected biodegradable reactant chemistries: a) open circuit potential and maximum power output measured over the range of one hour; and b) normalized cell polarization and power density curves measured at the time of peak power output.

species and supporting electrolytes are stored in the solid phase within the device. The concentration of OA is adjusted to 0.5 M in order to match the downstream neutralization requirement of the supporting electrolytes, since OA is a diprotic acid that can donate two protons per molecule. Therefore, 1 M KOH and 0.5 M OA can neutralize into neutral or near neutral conditions downstream after operation, and allow safe disposal. In this case, the cell contains 5.4 mg of pBQ and 22.5 mg of OA in the positive electrode compartment and 28 mg of KOH and either 11.4 mg of H_2BQS or 8.8 mg of AA in the negative electrode compartment. These masses are chosen to match the molar concentrations of active species and supporting electrolytes used in the previous section, for a total 1 mL of liquid (0.5 mL for each electrode), and are balanced for both downstream neutralization and the overall electrochemical reaction stoichiometry. Upon activation by the addition of 1 mL of DI-H_2O, the OCP of the cell is monitored for one hour as shown in Fig. 9a. It is shown that in the two cases of AA and H_2BQS, the capillary flow cell can hold the open circuit cell voltages of 1.1 V and 0.8 V respectively for more than one hour. This represents the functional time window of the device during which power can be generated and demonstrates that mixing of the two half-cell reactants progresses at a very slow pace despite their entry into a common absorbent pad. The initial progressive rise in the measured cell OCP curves is likely due to the transient nature of the device operation wherein the concentrations are not controlled and are based on the rates of species dissolution from the solid phase. Similarly, the slow decay in OCP after this initial period indicates the rate of reactant mixing in the device. The operational time of the battery is however expected to be reduced if the cell is continuously connected to an external load and will generate current until the redox species are fully discharged. Cell polarization curves are also measured at different instants during the functional time of the device. The maximum power output measured at different instants during the polarization curve measurements is shown in Fig. 9a, where it is seen that the cell with AA in the negative half-cell can provide a maximum power output of 1.9 mW (7.6 mW/cm^2) compared to 1.1 mW for the H_2BQS case. The full polarization and power density curves after 20 minutes of water activation, corresponding to the instant of maximum power, are given in Fig. 9b for both H_2BQS and AA cases. At the low current density range (< 4 mA/cm^2), the AA case shows higher activation over-potential when compared to the H_2BQS case, which confirms the slower kinetics in agreement with the findings in the previous sections. Despite this limitation, the cell with AA anode considerably outperforms the respective cell with H_2BQS anode at medium to high discharge current densities, reaching its peak power density of 7.6 mW/cm^2 at a current density of 18 mA/cm^2 (4.5 mA) compared to 4.4 mW/cm^2 at 12 mA/cm^2 (3 mA) for the latter case, which reflects the previous findings with the microfluidic cell. This discharge performance is considered sufficient to run a small measuring device or enable a wide range of other electronic components such as microprocessors, communication modules or displays.

While the data obtained with the microfluidic analytical cell show potential for higher power density outputs, the lower performance level obtained with the capillary flow cell can be attributed to the variation in the operating flow rates, internal cell resistance and the transient nature of reactant dissolution and transport. The present capillary flow cell prototype has not yet been optimized and further improvements are possible for the design and fluidics of the absorbent pads. Nonetheless, it is important to stress that a practical performance level has been achieved, meeting the requirements of single-use disposable applications. The results of this study thus provide the departing point for a new generation of biodegradable and sustainable power sources that minimize waste from conception and design. While the present work focuses on suitable organic species available off-the-shelf, the battery concept is not restricted to the use of these species. For example, many other suitable quinone species are commercially available and many more are under development by various groups. Custom species with tailored characteristics of solubility, redox state, redox potential and rate of dissolution can be synthesized by functionalizing quinone compounds.[52] This approach can enable higher cell voltages, power outputs and energy densities. While the present work demonstrated the use of oxalic acid and citric acid as organic supporting electrolytes, other inorganic acids may also be utilized such as phosphoric acid which exists as a solid powder in its pure form. This makes it suitable for storage and would ultimately form benign phosphate salts after device neutralization which are used as food additives or fertilizers. The present work also demonstrated the use of other organic redox compounds such as ascorbic acid. Various inorganic salts could also be used for this concept, which may enable high solubility as well as other environmental benefits. For example, Fe^{3+} is abundant and has a standard potential slightly higher than the pBQ used in this work (0.77 V vs. SHE)[60] and a relatively high aqueous solubility. Therefore, ferric salts of nitrates, sulfates or phosphates, that are known to enrich soils, may lead to a battery that could even add value to the soil or water in which it is disposed of.

Conclusions

This study reviewed the general requirements regarding solubility, biodegradability, storability in correct redox state, redox potential and kinetics of the reactant chemistries for biodegradable capillary flow batteries for single-use disposable applications. Mixed-media operation suitable for membrane-less cells was leveraged to allow direct use of commercially available organic compounds such as quinones by using an alkaline negative half-cell and an acidic positive half-cell with the added benefit of downstream neutralization for safe disposal. Prospective redox chemistries for each half-cell were systematically assessed by ex-situ measurements of solubility, redox potential and kinetics and in-situ discharge performance in a microfluidic co-laminar flow cell with flow through porous electrodes. An all-quinone cell comprising of LQ and pBQ for the negative and positive half-cells, respectively was shown to have a high open circuit potential of 1.24 V but was deemed unsuitable for disposable cells due to stability issues. The overall most effective chemistry identified for disposable cells was based on either ascorbic acid or H_2BQS in KOH and pBQ in oxalic acid at the negative and positive electrodes, respectively.

The coupling of these two half-cells in a microfluidic cell resulted in an open circuit cell voltage of 0.92 V and a peak power density of 42 mW/cm^2. Finally, the selected half-cell chemistries were demonstrated in a disposable capillary flow cell with all redox reactant and supporting electrolyte species stored in the solid phase on the device and dissolved upon water activation. The cell was shown to maintain high open circuit voltage for more than 1 hour and to achieve more than 2 mW peak power output at 4.5 mA which would be sufficient to power a wide variety of portable electronic components such as small signal processors, communication modules or displays. The results provide the departing point for a new generation of biodegradable and sustainable primary batteries that minimize waste from conception and design.

Acknowledgments

The funding for this research provided by the Electrochemical Society (ECS) and the Bill & Melinda Gates Foundation, as part of the Science for Solving Society's Problems Challenge (S^{3}P), is highly appreciated. Additional funding from Natural Sciences and Engineering Research Council of Canada (NSERC), Canada Foundation for Innovation (CFI) and British Columbia Knowledge Development Fund (BCKDF) is appreciated. J.P.E. thanks support from Marie Curie International Outgoing Fellowship (APPOCS) within the 7th European Community Framework. N. S. thank financial support received from ERC Consolidator grant (SUPERCELL). E.K. acknowledges support from the Canada Research Chairs program.

References

1. D. Lisbona and T. Snee, *Process Saf. Environ. Prot.*, **89**, 434 (2011).
2. L. Moreno-Merino, M. E. Jiménez-Hernández, A. de la Losa, and V. Huerta-Muñoz, *Sci. Total Environ.*, **526**, 187 (2015).
3. T. C. Wanger, *Conserv. Lett.*, **4**, 202 (2011).
4. D. Larcher and J. -M. Tarascon, *Nat. Chem.*, **7**, 19 (2015).
5. M. Sun, X. Yang, D. Huisingh, R. Wang, and Y. Wang, *J. Clean. Prod.*, **107**, 775 (2015).
6. W. McDonough and M. Braungart, *Cradle to cradle: Remaking the way we make things*, (2002).
7. Y. J. Kim, W. Wu, S. -E. Chun, J. F. Whitacre, and C. J. Bettinger, *Proc. Natl. Acad. Sci. U. S. A.*, **110**, 20912 (2013).
8. L. Yin, X. Huang, H. Xu, Y. Zhang, J. Lam, J. Cheng, and J. A. Rogers, *Adv. Mater.*, **26**, 3879 (2014).
9. M. Tsang, A. Armutlulu, A. W. Martinez, S. A. B. Allen, and M. G. Allen, *Microsystems Nanoeng*, **1**, 15024 (2015).
10. P. Nadeau, D. El-Damak, D. Glettig, Y. L. Kong, S. Mo, C. Cleveland, L. Booth, N. Roxhed, R. Langer, A. P. Chandrakasan, and G. Traverso, *Nat. Biomed. Eng.*, **1**, 0022 (2017).
11. C. Chen, Y. Zhang, Y. Li, J. Dai, J. Song, Y. Yao, Y. Gong, I. Kierzewski, J. Xie, and L. Hu, *Energy Environ. Sci.*, **10**, 538 (2017).
12. J. Maya-Cornejo, E. Ortiz-Ortega, L. Alvarez-Contreras, N. Arjona, M. Guerra-Balcazar, J. Ledesma-Garcia, and L. G. Arriaga, *Chem. Commun.*, **51**, 2536 (2015).
13. C. A. López-Rico, J. Galindo-De-La-Rosa, E. Ortiz-Ortega, L. Álvarez-Contreras, J. Ledesma-García, M. Guerra-Balcázar, L. G. Arriaga, and N. Arjona, *Electrochim. Acta*, **207**, 164 (2016).
14. E. Ortiz-Ortega, M. -A. Goulet, J. W. Lee, M. Guerra-Balcázar, N. Arjona, E. Kjeang, J. Ledesma-García, and L. G. Arriaga, *Lab Chip*, **14**, 4596 (2014).
15. J. P. Esquivel, F. J. Del Campo, J. L. Gómez de la Fuente, S. Rojas, and N. Sabaté, *Energy Environ. Sci.*, **7**, 1744 (2014).
16. S. O. Garcia, Y. V Ulyanova, R. Figueroa-Teran, K. H. Bhatt, S. Singhal, and P. Atanassov, *ECS J. Solid State Sci. Technol.*, **5**, M3075 (2016).
17. M. J. González-Guerrero, J. P. Esquivel, D. Sánchez-Molas, P. Godignon, F. X. Muñoz, F. J. del Campo, F. Giroud, S. D. Minteer, and N. Sabaté, *Lab Chip*, **13**, 2972 (2013).
18. Z. Zhu, T. Kin Tam, F. Sun, C. You, and Y. -H. Percival Zhang, *Nat. Commun.*, **5**, 877 (2014).
19. M. J. González-Guerrero, F. J. del Campo, J. P. Esquivel, D. Leech, and N. Sabaté, *Biosens. Bioelectron.*, **90**, 475 (2017).
20. J. W. Lee and E. Kjeang, *Biomicrofluidics*, **4**, 041301 (2010).
21. R. Ferrigno, A. D. Stroock, T. D. Clark, M. Mayer, and G. M. Whitesides, *J. Am. Chem. Soc.*, **124**, 12930 (2002).
22. E. R. Choban, L. J. Markoski, A. Wieckowski, and P. J. A. Kenis, *J. Power Sources*, **128**, 54 (2004).
23. M. A. Goulet and E. Kjeang, *J. Power Sources*, **260**, 186 (2014).
24. X. Lu, J. Xuan, D. Y. C. Leung, H. Zou, J. Li, H. Wang, and H. Wang, *J. Power Sources*, **314**, 76 (2016).
25. E. Kjeang, R. Michel, D. A. Harrington, N. Djilali, and D. Sinton, *J. Am. Chem. Soc.*, **130**, 4000 (2008).
26. M. -A. Goulet, O. A. Ibrahim, W. H. J. Kim, and E. Kjeang, *J. Power Sources*, **339**, 80 (2017).
27. T. H. Nguyen, A. Fraiwan, and S. Choi, *Biosens. Bioelectron.*, **54**, 640 (2014).
28. S. Choi, *Biotechnol. Adv.*, **34**, 321 (2016).
29. N. K. Thom, K. Yeung, M. B. Pillion, and S. T. Phillips, *Lab Chip*, **12**, 1768 (2012).
30. S. -S. Chen, C. -W. Hu, I. -F. Yu, Y. -C. Liao, and J. -T. Yang, *Lab Chip*, **14**, 2124 (2014).
31. Y. Koo, J. Sankar, and Y. Yun, *Biomicrofluidics*, **8**, 054104 (2014).
32. A. Zebda, L. Renaud, M. Cretin, F. Pichot, C. Innocent, R. Ferrigno, and S. Tingry, *Electrochem. commun.*, **11**, 592 (2009).
33. M. J. González-Guerrero, F. J. del Campo, J. P. Esquivel, F. Giroud, S. D. Minteer, and N. Sabaté, *J. Power Sources*, **326**, 410 (2016).
34. A. Fraiwan, H. Lee, and S. Choi, *IEEE Sens. J.*, **14**, 3385 (2014).
35. A. Fraiwan and S. Choi, *Phys. Chem. Chem. Phys.*, **16**, 26288 (2014).
36. C. Fischer, A. Fraiwan, and S. Choi, *Biosens. Bioelectron.*, **79**, 193 (2016).
37. H. Lee and S. Choi, *Nano Energy*, **15**, 549 (2015).
38. Z. Song, T. Ma, R. Tang, Q. Cheng, X. Wang, D. Krishnaraju, R. Panat, C. K. Chan, H. Yu, and H. Jiang, *Nat. Commun.*, **5**, 273 (2014).
39. Z. Song, X. Wang, C. Lv, Y. An, M. Liang, T. Ma, D. He, Y. -J. Zheng, S. -Q. Huang, H. Yu, and H. Jiang, *Sci. Rep.*, **5**, 10988 (2015).
40. K. K. Fu, Z. Wang, C. Yan, Z. Liu, Y. Yao, J. Dai, E. Hitz, Y. Wang, W. Luo, Y. Chen, M. Kim, and L. Hu, *Adv. Energy Mater.*, **6**, 1502496 (2016).
41. J. P. Esquivel, P. Alday, O. A. Ibrahim, B. Fernandez, E. Kjeang, and N. Sabaté, *Adv. Energy Mater.*, **Accepted**, 1700275 (2017).
42. O. A. Ibrahim, M. A. Goulet, and E. Kjeang, *Electrochim. Acta*, **187**, 277 (2016).
43. O. A. Ibrahim, M. -A. Goulet, and E. Kjeang, *J. Electrochem. Soc.*, **162**, F639 (2015).
44. G. L. Soloveichik, *Chem. Rev.*, **115**, 11533 (2015).
45. J. Marschewski, L. Brenner, N. Ebejer, P. Ruch, B. Michel, D. Poulikakos, X. Li, Y. -B. Zhang, J. Jiang, O. M. Yaghi, and E. N. Wang, *Energy Environ. Sci.*, **10**, 780 (2017).
46. J. Winsberg, T. Hagemann, T. Janoschka, M. D. Hager, and U. S. Schubert, *Angew. Chemie - Int. Ed.*, **56**, 686 (2016).
47. B. Huskinson, M. P. Marshak, C. Suh, S. Er, M. R. Gerhardt, C. J. Galvin, X. Chen, A. Aspuru-Guzik, R. G. Gordon, and M. J. Aziz, *Nature*, **505**, 195 (2014).
48. B. Yang, L. Hoober-Burkhardt, F. Wang, G. K. Surya Prakash, and S. R. Narayanan, *J. Electrochem. Soc.*, **161**, A1371 (2014).
49. K. Lin, Q. Chen, M. R. Gerhardt, L. Tong, S. B. Kim, L. Eisenach, A. W. Valle, D. Hardee, R. G. Gordon, M. J. Aziz, and M. P. Marshak, *Science*, **349**, 1529 (2015).
50. K. Wedege, E. Dražević, D. Konya, and A. Bentien, *Sci. Rep.*, **6**, 39101 (2016).
51. J. B. Conant and L. F. Fieser, *J. Am. Chem. Soc.*, **46**, 1858 (1924).
52. S. Er, C. Suh, M. P. Marshak, and A. Aspuru-Guzik, *Chem. Sci.*, **6**, 845 (2015).
53. F. J. Enguita and A. L. Leitão, *Biomed Res. Int.*, **2013**, 1 (2013).
54. US EPA, *Estim. Programs Interface Suite Microsoft Wind. (EPISuite), v 4.11* (2016).
55. Y. Xu, Y. H. Wen, J. Cheng, G. P. Cao, and Y. S. Yang, *Electrochim. Acta*, **55**, 715 (2010).
56. G. Atkinson and W. McBryde, *Can. J. Chem.*, **35**, 477 (1957).
57. B. Yang, L. Hoober-Burkhardt, S. Krishnamoorthy, A. Murali, G. K. S. Prakash, and S. R. Narayanan, *J. Electrochem. Soc.*, **163**, A1442 (2016).
58. P. S. Guin, S. Das, and P. C. Mandal, *Int. J. Electrochem.*, **2011**, 1 (2011).
59. M. Quan, D. Sanchez, M. F. Wasylkiw, and D. K. Smith, *J. Am. Chem. Soc.*, **129**, 12847 (2007).
60. W. M. Haynes, *CRC Handbook of Chemistry and Physics*, 94th Edition, (2013).
61. M. Rafiee and D. Nematollahi, *Electroanalysis*, **19**, 1382 (2007).
62. J. Du, J. J. Cullen, and G. R. Buettner, *Biochim. Biophys. Acta - Rev. Cancer*, **1826**, 443 (2012).
63. N. Fujiwara, S. Yamazaki, Z. Siroma, T. Ioroi, and K. Yasuda, *J. Power Sources*, **167**, 32 (2007).
64. C. Giacomelli, K. Ckless, D. Galato, F. S. Miranda, and A. Spinelli, *J. Braz. Chem. Soc.*, **13**, 332 (2002).
65. S. I. Bailey and I. M. Ritchie, *Electrochim. Acta*, **30**, 3 (1985).
66. R. Gulaboski, I. Bogeski, V. Mirčeski, S. Saul, B. Pasieka, H. H. Haeri, M. Stefova, J. P. Stanoeva, S. Mitrev, M. Hoth, and R. Kappl, *Sci. Rep.*, **3**, 2841 (2013).
67. C. A. Martínez-Huitle, S. Ferro, and A. De Battisti, *Electrochim. Acta*, **49**, 4027 (2004).